

RESEARCH ARTICLE

Benchmarking of tools for axon length measurement in individually-labeled projection neurons

Mario Rubio-Teves¹✉, Sergio Díez-Hermano²✉, César Porrero¹, Abel Sánchez-Jiménez², Lucía Prensa¹, Francisco Clascá¹, María García-Amado¹‡, José Antonio Villacorta-Atienza²*✉

1 Department of Anatomy & Neuroscience, School of Medicine, Autónoma de Madrid University, Madrid, Spain, **2** Department of Biodiversity, ecology and evolution, Biomathematics Unit, Faculty of Biology, Complutense University of Madrid, Madrid, Spain

✉ These authors contributed equally to this work.

‡ MG-A and JAV-A also contributed equally to this work.

* josea@ucm.es



OPEN ACCESS

Citation: Rubio-Teves M, Díez-Hermano S, Porrero C, Sánchez-Jiménez A, Prensa L, Clascá F, et al. (2021) Benchmarking of tools for axon length measurement in individually-labeled projection neurons. *PLoS Comput Biol* 17(12): e1009051. <https://doi.org/10.1371/journal.pcbi.1009051>

Editor: Marcus Kaiser, University of Nottingham, UNITED KINGDOM

Received: April 29, 2021

Accepted: November 19, 2021

Published: December 8, 2021

Copyright: © 2021 Rubio-Teves et al. This is an open access article distributed under the terms of the [Creative Commons Attribution License](https://creativecommons.org/licenses/by/4.0/), which permits unrestricted use, distribution, and reproduction in any medium, provided the original author and source are credited.

Data Availability Statement: Neuron accession numbers and code used for running experiments, model fitting, plotting and statistical analysis is available on the free-access repository: https://gin.g-node.org/sergio.dh/Rubio_et_al_2021.

Funding: This study was supported by the following grants: European Union's Horizon 2020 Research and Innovation Program, European Commission https://ec.europa.eu/info/index_en (Grant Agreement No. 945539 - HBP SGA3, to MR, MG, CP, LP, FC); Ministerio de Ciencia e

Abstract

Projection neurons are the commonest neuronal type in the mammalian forebrain and their individual characterization is a crucial step to understand how neural circuitry operates. These cells have an axon whose arborizations extend over long distances, branching in complex patterns and/or in multiple brain regions. Axon length is a principal estimate of the functional impact of the neuron, as it directly correlates with the number of synapses formed by the axon in its target regions; however, its measurement by direct 3D axonal tracing is a slow and labor-intensive method. On the contrary, axon length estimations have been recently proposed as an effective and accessible alternative, allowing a fast approach to the functional significance of the single neuron. Here, we analyze the accuracy and efficiency of the most used length estimation tools—design-based stereology by virtual planes or spheres, and mathematical correction of the 2D projected-axon length—in contrast with direct measurement, to quantify individual axon length. To this end, we computationally simulated each tool, applied them over a dataset of 951 3D-reconstructed axons (from [NeuroMorpho.org](https://neuro-morpho.org/)), and compared the generated length values with their 3D reconstruction counterparts. The evaluated reliability of each axon length estimation method was then balanced with the required human effort, experience and know-how, and economic affordability. Subsequently, computational results were contrasted with measurements performed on actual brain tissue sections. We show that the plane-based stereological method balances acceptable errors (~5%) with robustness to biases, whereas the projection-based method, despite its accuracy, is prone to inherent biases when implemented in the laboratory. This work, therefore, aims to provide a constructive benchmark to help guide the selection of the most efficient method for measuring specific axonal morphologies according to the particular circumstances of the conducted research.

Innovación (Spanish Ministry of Science and Innovation) <https://www.ciencia.gob.es/>, FLAG-ERA grant NeuronsReunited, grant number: PCI2019-111900-2 to MR, MG, CP, LP, FC; Ministerio de Ciencia e Innovación grant number: BFU2017-88549 to MR, MG, CP, LP, FC; Fundación Bancaria “la Caixa” <https://fundacionlacaixa.org/es/> Grant number: 100010434 to SDH. The funders had no role in study design, data collection and analysis, decision to publish, or preparation of the manuscript.

Competing interests: The authors have declared that no competing interests exist.

Author summary

Characterization of single neurons is a crucial step to understand how neural circuitry operates. Visualization of individual neurons is feasible thanks to labelling techniques that allow precise measurements at cellular resolution. This milestone gave access to powerful estimators of the functional impact of a neuron, such as axon length. Although techniques relying on direct 3D reconstruction of individual axons are the gold standard, handiness and accessibility are still an issue. Indirect estimations of axon length have been proposed as agile and effective alternatives, each offering different solutions to the accuracy-cost tradeoff. In this work we report a computational benchmarking between three experimental tools used for axon length estimation on brain tissue sections. Performance of each tool was simulated and tested for 951 3D-reconstructed axons, by comparing estimated axon lengths against direct measurements. Assessment of suitability to different research and funding circumstances is also provided, taking into consideration factors such as training expertise, economic cost and required equipment, alongside methodological results. These findings could be an important reference for research on neuronal wiring, as well as for broader studies involving neuroanatomical and neural circuit modelling.

This is a *PLOS Computational Biology* Benchmarking paper.

Introduction

The highly integrated functioning of the brain relies on axons that directly connect distant regions. The introduction in the past decade of new viral vectors able to drive the in vivo expression of high levels of marker proteins has allowed, for the first time, the consistent and complete visualization of such long-range projection axons with single-cell resolution [1–6]. Studies in small rodent brains applying these methods have revealed that despite being submicron-thick, an individual neuron axon can extend over long distances and branch in complex and specific patterns [6–9].

Unlike dendrites, which integrate input signals [10–12], the axon is a transmission compartment for all-or-none fast action potentials. The functional impact of signals travelling down an axon thus depends critically on the wiring of the axon, as it constrains the number and distribution of its synapses. Axon morphologies may in this way lead to different network configurations, so precise axon characterization is a must for modelling and describing a plethora of brain capabilities [13–15]. Interestingly, the number and distribution of synapses can be reliably derived from the axon length within its target structures [8,9,16]. Accurate measurement of axon length, therefore, is key for the functional modelling of brain-wide circuits as it estimates the functional impact of the single neuron [17,18].

However, mapping and measuring long-range projection axon trees remains challenging, as it requires working across a wide range of spatial scales, from submicron to brain-wide [19]. A significant recent advance has been the development of automated platforms that combine serial sectioning with high-resolution confocal image acquisition to produce massive whole-brain volumetric image datasets. On these datasets, fluorescently tagged axons can be traced and measured using tools for 3D navigation and annotation. Deformation of these datasets is known and measurable, and the axon length measurements are thus reliable as far as the

reconstructions are complete. Nevertheless, devices for producing high-resolution 3D datasets are prohibitively expensive and the resulting multi-terabyte datasets require high-end computing infrastructure. For the foreseeable future, these high-end platforms will remain limited to industrial-scale research facilities. At present they remain focused in producing open-access datasets of adult “standard” model species brains intended as reference for other brain circuit studies [6,20–22].

Hundreds of laboratories and imaging facilities around the world currently rely on small, camera-lucida (2D) or computerized (3D) systems to reconstruct and measure neuron morphologies from brain tissue sections [23–25]. These systems remain the feasible way for reconstructing neuronal morphologies on brains manipulated under specific experimental conditions, or when in situ visualization of specific tissue markers is required, in developing animals or in species other than mice. However, producing accurate axon length data from serial histological sections is not trivial, as projection axons can extend across the brain and thus be spread over a large number of tissue sections. Thus, it is important to evaluate the accuracy and efficiency of the procedures currently in use, with the aim of comparing data available in the literature from different methods.

Direct measurements of axon length can be obtained through three-dimensional (3D) reconstruction-tracing of arborizations across serial sections [26]. This is usually done manually and is slow and work-intensive, as it must be done at high magnification and deals with uneven distortions and misalignments due to histological tissue processing. A widely used computerized tool is NeuroLucida (MBF Bioscience, Williston, VT, USA), which allows for manual tracing among other capabilities, but a wide array of software tools from different sources is also available online [24]. Regardless of how sophisticated the software used is, the basis for length estimation is still the same: transforming image data into a series of vectors with a tree-like structure defined by a set of parameters that includes its euclidean coordinates, from which an approximation to the real, total path length is derived.

A faster, indirect alternative is to produce a 2D reconstruction by projecting onto a plane using a camera lucida or a slide-scanner, and then multiplying it by a correction factor [2,7]. Although this method has been recently applied to a wide range of thalamocortical neurons, the accuracy of the estimation method and the suitability of the correction factor has not been tested before.

Other indirect approaches to measure axon length are based on stereological techniques. Design-based stereology takes advantage of unbiased sampling schemes with different kinds of probes (planes or spheres) that are applied to the tissue to produce a number of interactions with the object of interest (the axon) that, because of the randomness of the sampling, can be used to mathematically infer its length with a known error [27–29]. These stereological methods have been traditionally applied to estimate the axonal length of neuronal populations ([30,31] for virtual planes; [32–34] for virtual spheres) and, more recently, of individual neurons [35].

In the present study, we sought to compare these estimation tools when measuring individual highly complex axonal arbors. This way, we propose a twofold objective. On the one hand, we assess the accuracy and efficiency of these methods to provide a rigorous rationale of their pros and cons. On the other hand, we evaluate their performance when estimating individual axon length and so as a qualitative approach to the functional importance of a single neuron. Taking advantage of the large number of neuron morphologies available at NeuroMorpho.org [36], we computationally implemented length estimation protocols from model-based estimates (mathematical correction of 2D length) and design-based stereology (sampling with isotropic virtual planes and spheres) to compare among themselves and with direct reconstruction-derived measurements. Our results provide: 1) a classification of the different

estimation methods according to their accuracy and performing effort, 2) a guide for selecting the most suitable parameters for each length estimation method in line with the researcher's necessities (type of axon characterization demanded by the problem, available funding and personnel, assumable error, time to be invested, etc.) and 3) a summary of advantages and disadvantages of estimates vs. direct methods.

Materials and methods

Ethics statement

All procedures involving live animals were conducted under protocols approved by the University ethics committee and the competent Spanish Government agency (PROEX 175/16), in accordance with the European Community Council Directive 2010/63/UE. The soma of these neurons was located in the thalamus, and their axon extended to different targets in the cerebral cortex.

Neuron sample

A sample of 951 neuron morphology files was downloaded from the NeuroMorpho database (NeuroMorpho.Org, RRID:SCR_002145; [36]).

We searched the database for full-morphology files produced on the mouse model (*Mus musculus*). The neurons contained in those files had been uploaded to NeuroMorpho.org by a number of different laboratories, and were produced either through direct reconstruction on a series of sections from a sparsely-labeled brain (containing one or a few neurons) that spanned the total length of the arbor or, in the case of those belonging to the MouseLight project, through semiautomatic tracing of single cells from a densely labeled (containing hundreds of neurons) brain digitally scanned by means of single two-photon tomography (STPT) [4]. Although different in practice, these two technical approaches are conceptually the same and were considered equivalent in the coming analysis. That is, the axonal length of the 3D reconstructions was considered as the “true value” and used to measure the accuracy of the different estimations.

Neurons were then qualitatively classified into four distinct classes based on easily recognizable features of their axonal morphology, following the same criteria that has been recently used to classify thalamic projection neurons [37] (Fig 1). The axon of class 1 (“focal”) neurons arborizes in a single and distant spot (N = 90). The axon of class 2 (“multi-focal”) neurons arborizes in several distant and separate regions (N = 116). The axon of class 3 (“disperse”) neurons arborizes over a large region in a more sparse manner (N = 269). Lastly, the axon of class 4 (“local”) neurons arborizes in the immediate vicinity of the soma (N = 476). Some neurons had intermediate characteristics that could cause them to be assigned to more than one category. In those cases, the most predominant feature regarding the number of focal clusters or axonal dispersion, decides what class it belongs to. This classification pays no attention to the anatomical position or developmental origin of each cell, and was performed previous to the analysis in order to see if gross morphological appearance of the axon could be used to infer the applicability of a specific method to a particular neuron.

Computational implementation of axon length estimation methods

The full-morphology files from the database were analyzed by means of custom-made Matlab scripts (Matlab 2017b; The Mathworks, Natick, MA, USA), where only the information for the axon was treated. Projection-based method was implemented by eliminating the Z coordinates from the axon points to project them onto the XY plane. The length of the resulting projected

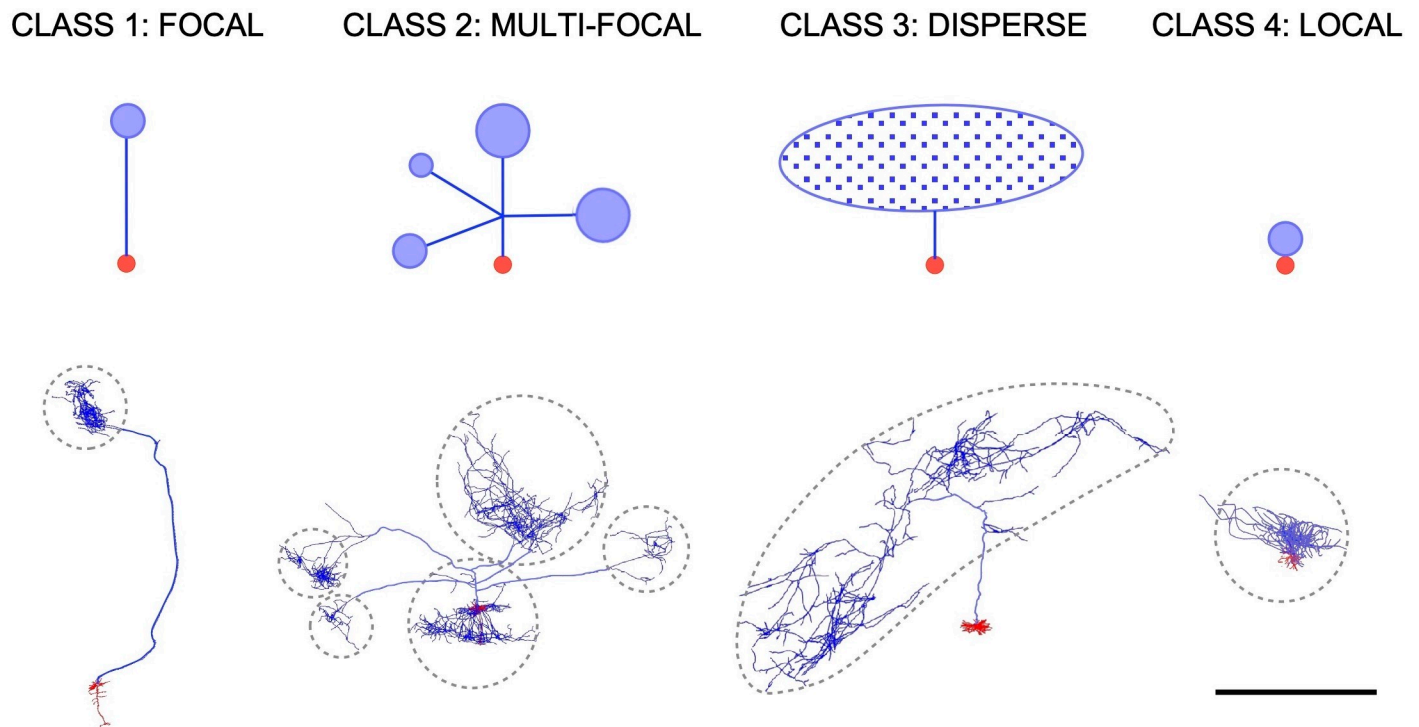


Fig 1. Neuron classification. **Top.** Schematic diagrams of the four neuronal classes defined in the study. Red circles represent the somatodendritic domain. Blue lines in class 1, class 2 and class 3 schemes represent the main axon trunk and collateral branches. Blue circles in class 1, class 2 and class 4 represent focal terminal arborizations of the axon. Blue oval filled with dots in class 3 represents a large and sparse axonal arborization. **Bottom.** One representative example of each neuronal class extracted from the NeuroMorpho dataset (Drawings generated from morphologies AA0641, AA0002, AA0051, AA0771 from Neuromorpho.org). Axon is represented in blue whereas dendrites and soma are depicted in red. Dashed contours enclose the spatial extent of the axonal arborizations. Scale bar, 1 mm.

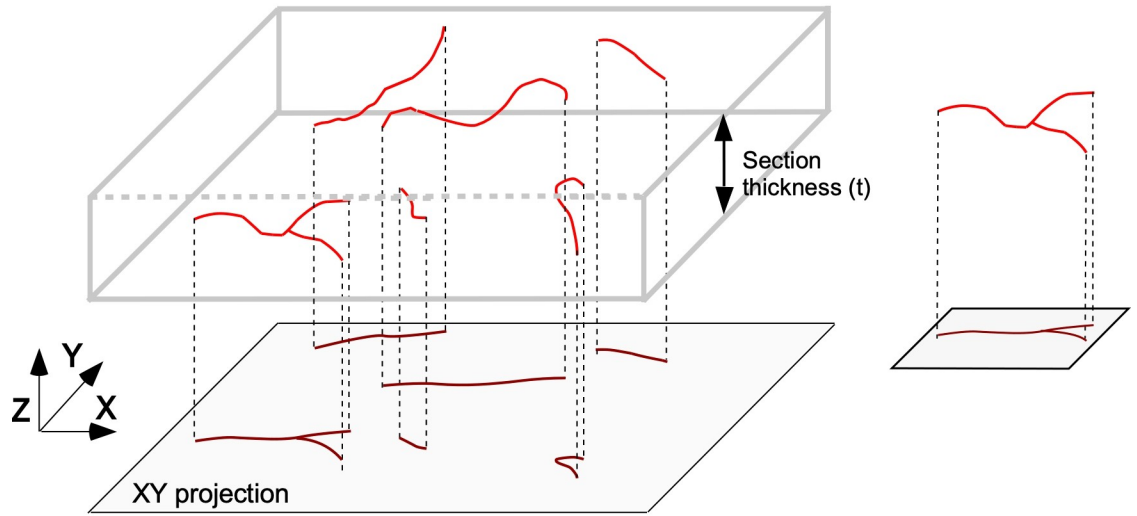
<https://doi.org/10.1371/journal.pcbi.1009051.g001>

axon multiplied by a proper coefficient (see [Results](#)) will then be used as estimation of the axon tridimensional length. Note that the XY plane was not *a priori* established but defined by its own morphology file and each source's method of acquisition. Sphere and plane-based estimation methods were implemented following similar processes. The analyzed axon was divided into sections 50 μm thick parallel to the XY plane (plane defined by X and Y coordinates in the morphology file). In both cases the sampling box dimensions were 50x50x50 μm^3 and all sections were analyzed. The specific probes (spheres and planes) were introduced into the sampling box according to the requirements of each particular method (for the plane-based method all of the planes in each sampling box had the same orientation, which varied randomly between boxes). The relevant parameters, as sphere diameter, plane distance, and step length between sampling boxes, were adjusted accordingly for the computational simulations ([Fig 2](#)).

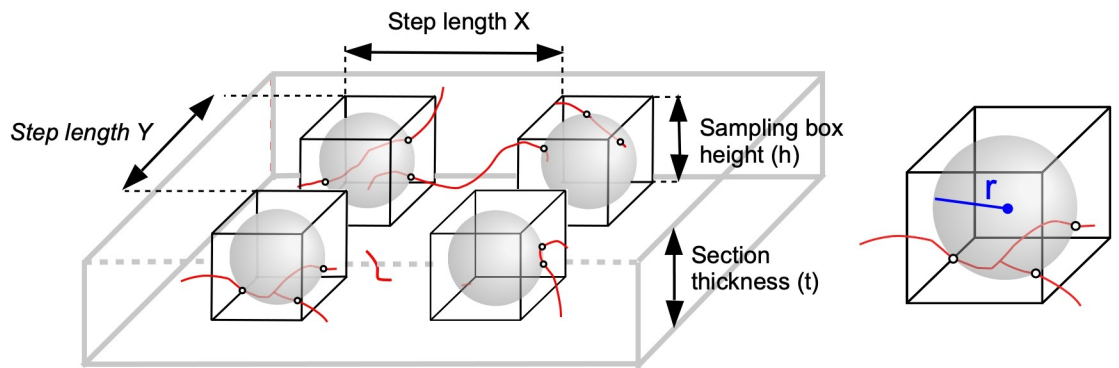
Statistical analysis

Projection-based length estimation. Correlation between axon's real length and projection's length was assessed by means of linear regression (ordinary least squares, OLS), with axon class considered as a factor. Parameter estimators (alphas) were obtained through error-resampling bootstrapping (2000 repetitions). 95% confidence intervals (CI95%) were calculated using the 0.025 (lower limit) and 0.975 (upper limit) quantiles of the bootstrapped distribution of alpha values. Prediction errors were estimated through 5-fold cross validation (CV), independently for every axon class and plane combination. Error's density distributions were

A PROJECTIONS



B VIRTUAL SPHERES



C ISOTROPIC VIRTUAL PLANES

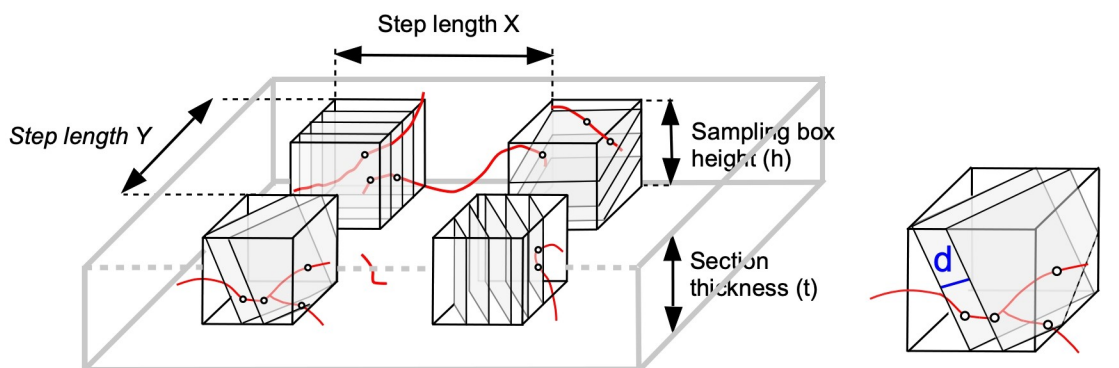


Fig 2. Methods for length estimation. **A.** Projections method. One tissue section containing several axon fibers (above). The method consists of measuring the axon length projected in the X-Y plane (represented below) and multiplying it by a factor to obtain the 3D actual length. **B.** Stereology with virtual spheres. This method is based on the estimation of axonal length from the intersections occurring between the axon segments and the surface of virtual spheres introduced in sampling boxes inside the tissue section thickness. Four sampling boxes inside a section are represented in black, with the virtual spheres inside (in grey). **C.** Stereology with virtual planes estimates axonal length by using the intersections between the axon segments (in red) and a set of parallel and isotropically oriented planes contained within the sampling boxes included in the tissue sections. Four sampling boxes (in black) with parallel virtual planes inside (in grey) are represented; r and d stand respectively for sphere radius and distance between planes.

<https://doi.org/10.1371/journal.pcbi.1009051.g002>

obtained through bootstrapping (100 repetitions), and probabilities were calculated as the area under the curve for a given error interval (i.e. + 5% and +10%). Tuning of hyper-parameters such as bootstrapping steps followed convergence to a stop-criteria (error gain below 0.1%).

3d plane-based stereology. Model errors were calculated as the absolute difference between axon's real length and length estimated by all combinations of sampling step and distance between planes. Correlation between model error, step and distance was assessed by means of linear regression (OLS), independently for every axon class. Prediction errors were calculated as smoothed interpolations for 200 possible values of step and distance. Error's density distributions were obtained as smoothed histograms with automatic bandwidth selection, and probabilities were calculated as the area under the curve for every step and distance combination and for a given error interval (i.e. + 5% and +10%). Additionally, all models defined by step and distance were compared in terms of normalized root mean square error (RMSE) by means of 5-fold CV.

3d sphere-based stereology. Analysis followed the same procedures as the plane-based stereology, considering sampling step and probe diameters in this case.

Mean absolute error, mean intersections, and error probability distributions were obtained through linear interpolation from these estimations performed for diameter values in 10, 15, 20, . . ., 50 (virtual spheres), distance values in 3, 6, 9, . . ., 30 (virtual planes) and step values in 70, 80, . . ., 150 (both probe types). The adjusted R-squared coefficients range from 0.88 to 0.98. In both spheres and planes approaches, accuracy of the mean error estimation was obtained as the upper limit of the confidence interval at 95% confidence.

Practical implementation. We performed practical examples with real tissue sections comparing the three methods analyzed in the computational approach: direct axon measurements from Neurolucida reconstructions, projections-based length estimation and design-based stereology (virtual planes) (Fig 2).

Single thalamocortical neurons were transfected with an RNA construct driving the expression of a fluorescent protein eGFP fused with a palmytoilation signal GAP43 under the Sindbis viral subgenomic promoter (Sind-Pal-eGFP; [1]). Transfections were performed following a previously described method of in vivo RNA electroporation [5]. Briefly, borosilicate micropipettes (20- μ m tip) were backfilled with an RNA solution (1.8 μ g/ μ L) in a high-saline vehicle (NaCl 0.5 M) and mounted on a holder equipped with a pressure port and an electrode. The micropipette tip was stereotaxically positioned into either the ventral posteromedial nucleus (VPM), the posterior nucleus (Po), the lateral geniculate nucleus (LGN) or the lateral posterior (LP) of the mouse thalamus, and 50–100 nL of the RNA solution were injected using a precision electro-valve system (Picospritzer II, Parker Hannifin, Cleveland OH). Two to four 200 Hz trains of 1-ms negative-square pulses at 50 V were applied using a CS20 stimulator (Cibertec, Madrid, Spain). After 52–65 h survival, animals were transcardially perfused with 4% PFA in PB 0.1M, pH 7.4, for 8 min and cryoprotected in a sucrose solution (30% in PB) overnight. Serial 50 μ m-thick coronal sections were obtained using a freezing microtome (Leica Microsystems). To visualize eGFP labeling, free-floating sections were incubated in rabbit anti-GFP

serum (1:500; EXBIO), followed by incubation with a biotinylated goat anti-rabbit serum (1:100; Sigma-Aldrich). Sections were then processed using avidin-biotin-peroxidase kit (ABC; 1:100; Vectastain Elite, Vector Laboratories, Burlingame, CA, USA) and diaminodiaminobenzidine–glucose oxidase with nickel enhancement. Finally, all sections were serially mounted onto gelatin-coated glass slides, air-dried, lightly counterstained with thionin, dehydrated, and coverslipped with DePeX (Serva Electrophoresis).

We measured the axonal length of six mouse thalamocortical neurons which fitted in classes 1 (one neuron from the VPM and one from the LGN), 2 (three neurons from Po), and 3 (one neuron from the LP) of our study by using the mentioned three length estimation methods (Fig 3). We did not include class 4 neurons in the experimental approach based on the results obtained with the computational approach (see Results section). The complete axon inside the cortex was reconstructed using the NeuroLucida software (NeuroLucida 2020; MBF Bioscience, Williston, VT, USA) and the length obtained with this direct measurement was compared with the resulting axonal length from both the use of virtual planes (stereology) or the projections method. We used 50 microns-thick sections containing the complete axon of each neuron.

The projection-based method consisted in drawing the complete axon of each neuron, contained in the corresponding set of sections, by using the 20X lens of a microscope connected to a camera lucida (Nikon Eclipse E400; Nikon, Tokyo, Japan). Camera lucida drawings containing the projected axon were scanned and redrawn for digitization on Canvas X GIS (Canvas GFX, Boston, MA, USA); this software was also used to extract the length of all axon segments. Projected length was multiplied by the proper alpha value of each axon class (see Fig 4B and “Projected based estimation” section) to estimate the real axonal length.

The stereological approach consisted on projecting virtual planes over the sections observed in a microscope connected to a computer running stereology software (newCAST stereology software package for VIS; Visiopharm, Denmark); sampling parameters used for the 3 neuron classes were: 75 μm step length in X and Y axes; sampling box size: 50 (X axis), 50 (Y axis) and 10 (Z axis) μm and 5 μm of plane separation; a fractionator sampling scheme was used to estimate the axonal length [38]. We calculated the coefficient of error (CE) due to the sampling method for the estimates by using the equations detailed in [39].

Results

Projection-based estimation

The projection-based method of length estimation relies on the assumption of isotropy (that fibers distribute their length equally across all possible directions; [23]). Under this condition the 3D length of isotropic fibers is equal to the product of the two-dimensional (2D) length of its projection onto a plane by a constant factor of $\pi/2$ (Fig 2A). However, neurons do not distribute their fibers randomly, so the accuracy of this estimation will ultimately depend on the degree of anisotropy of the cell it is being applied to. Another way of seeing this is that each neuron will have its own correction factor, depending on its degree of anisotropy.

In order to analyze the reliability of projection-based axon length estimation in real neurons, we projected the morphologies of the dataset from [NeuroMorpho.org](https://neuro-morpho.org) onto the XY, XZ and YZ planes. We found that the relationship between the 2D projection length and the reference length of the 3D model is indeed linear for all four classes of neurons (Fig 4A). This confirms there is a coefficient describing the relationship between the 3D length of the real structure and the length of its projection onto a plane. For the dataset used in this study, we calculated the alpha values for the different classes of axons in our classification, whose 95% confidence intervals (95% CI) overlap between 1.272 and 1.277 (Fig 4B). This interval encloses the theoretical value of $4/\pi$ (≈ 1.273), which is the ratio between the axon length in the 3D

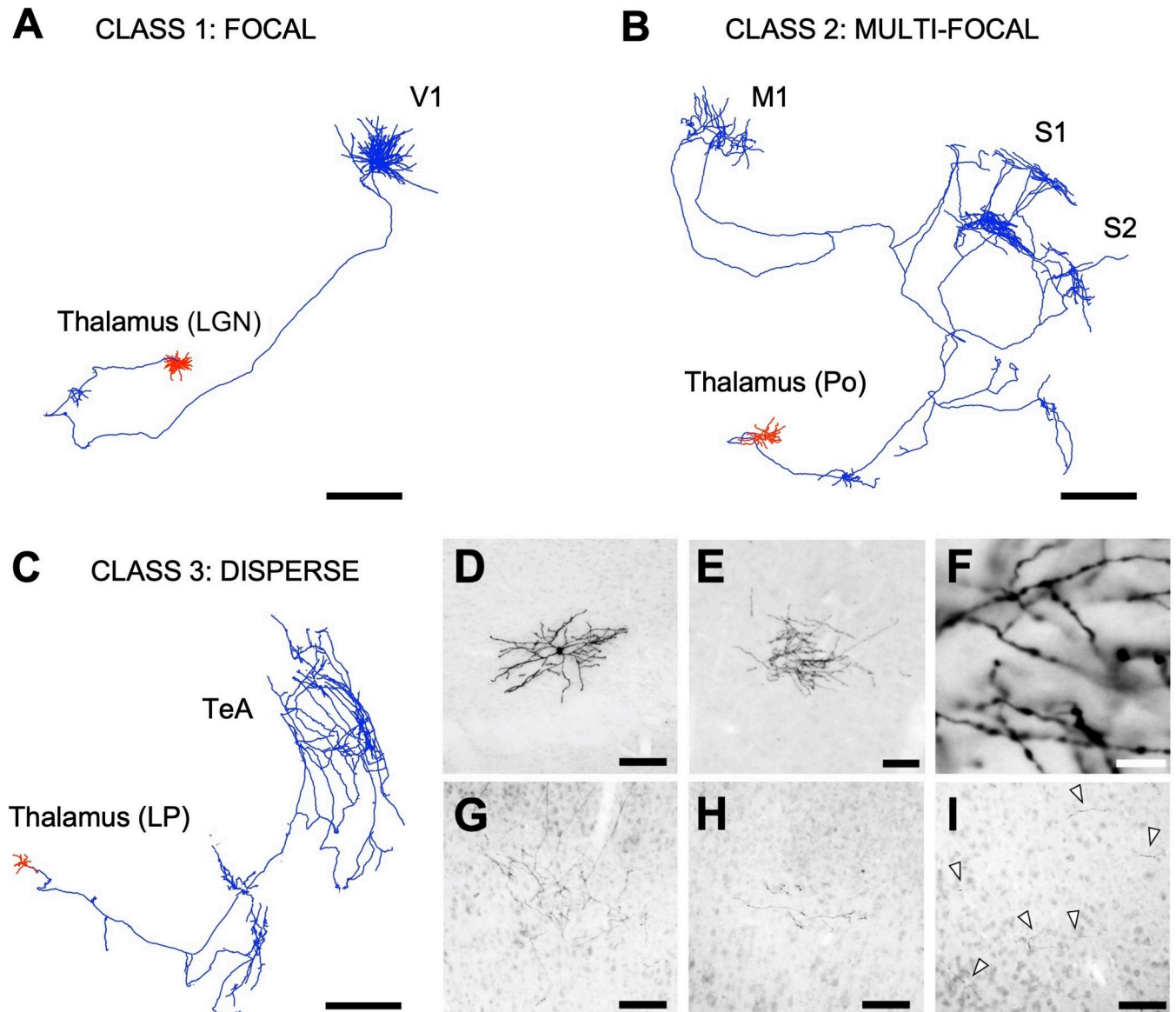


Fig 3. Reconstruction of the complete axonal (blue) and dendritic (red) trees of 3 individually-labelled thalamocortical neurons used for the practical implementation of the length estimation methods in the laboratory. A. Class 1 neuron from the lateral geniculate nucleus (LGN) arborizing focally in primary visual cortex (V1). B. Class 2 neuron from the posterior nucleus (Po) arborizing focally in 3 separate cortical areas: primary motor cortex (M1), primary somatosensory cortex (S1) and secondary somatosensory cortex (S2). C. Class 3 neuron from the lateral posterior nucleus (LP) arborizing over a large extension of the temporal association cortex (TeA). D-I. Brightfield microscope images of 50 μm thick coronal sections showing different parts of the labeled neurons after immunostaining for GFP and ABC-DAB-Nickel intensification. D. Cell body and dendrites of a Class 1 neuron. E. Axonal arborization in the cortex of a Class 1 neuron. F. High-magnification details of the axonal branches shown in E. G-H. Axonal arborizations of the Class 2 neuron in the motor cortex (G) and the primary somatosensory cortex (H). I. Axonal arborization in the temporal cortex of the Class 3 neuron. Note the sparse distribution of the axonal fragments (Arrowheads). Scale bars: A-C, 500 μm ; D, E, G, H, I, 100 μm ; F, 10 μm .

<https://doi.org/10.1371/journal.pcbi.1009051.g003>

space and the length of its planar projection under zero-anisotropy assumption (S1 Text). The particular alpha values for each axon class are detailed in Fig 4A.

Next, we quantified the probability of estimation error, defined as the difference between the 3D axon length and the length estimated from the model, when the different alpha factors are applied to the corresponding axon class in the projection-based approach. In order to do that, all axons were projected onto XY, XZ and YZ planes and their 3D length were estimated

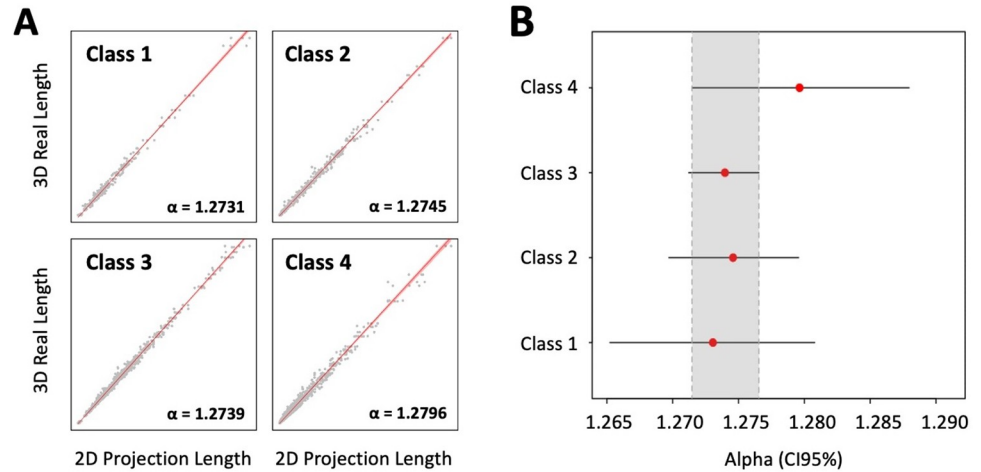


Fig 4. Axon length correlations for projection-based stereology. **A.** Correlation between 3D real length and 2D projection length, by axonal class. Red lines represent the mean estimated 3D real length (ordinary least squares), and light red shaded areas correspond to 95% confidence intervals (CI95%). Gray dots depict full samples comprising all planes measurements (XY, XZ and YZ, note the organization of the data in triplets). Global adjusted R-squared = 0.99. **B.** Estimated slopes (red dots) and CI95% (horizontal black bars) values for correlations in A. Slopes can be interpreted as coefficients (alpha) that multiply 2D projection values to obtain predictions of 3D real lengths. Note that all axon classes share a common set of potential alphas at a 95% confidence level (gray shaded area).

<https://doi.org/10.1371/journal.pcbi.1009051.g004>

by multiplying the projection length by alpha. The area under curves in Fig 5A describes the probability of finding a specific estimation error; as an example, dark and lightly shaded areas correspond to the probability of getting an estimation error of 5 and 10%, respectively. Noticeably, these cover much of the area under the curve, which means that it is highly probable to get estimation errors lower than 10% when using this approach. Specifically (Fig 5B), classes 1, 2, 3 and 4 neurons had a 65, 78, 71 and 38% probability of having a 5% absolute estimation error (estimation error between -5% and 5%), whereas the probability of it being 10% was 88, 92, 88 and 62%, respectively. It should be remarked that these estimation errors were similar

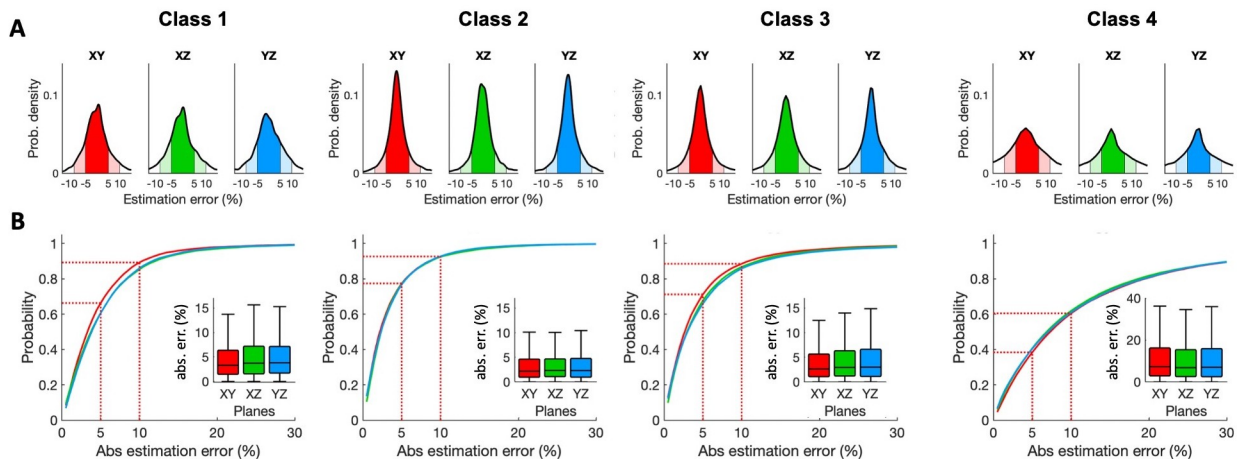


Fig 5. Estimation error probability projection-based stereology. **A.** Estimation error is distributed according to the shown probability densities (axon classes in columns; red, green, and blue for XY, XZ, and YZ planes respectively). The probability of getting a certain error during axon length estimation will be given by the area below the curves (dark and light colors for + 5% and + 10% estimation error respectively). **B.** Absolute estimation error vs. probability (given by the area below the curves in A). Dashed lines point the probabilities of estimating axon length with absolute errors of 5% and 10%, (colored areas in A). Insets. Absolute error distributions for planes XY, XZ, and YZ.

<https://doi.org/10.1371/journal.pcbi.1009051.g005>

across orthogonal projection planes, showing the robustness of the method when applied in practice since the projection plane is not a relevant parameter.

Stereological sampling with virtual spheres to estimate 3D length

In order to attain an unbiased stereological estimate, every object (whose length will be estimated) in the specimen has to have the same probability of being sampled. In the case of length estimates, 2D probes (surfaces) are used to scan the sample volume. The object length is thus estimated by quantifying the intersections between the object and the probe, whose position and orientation must be random to ensure an unbiased estimation. The stereological sampling scheme [28] draws on the inherent advantages of virtual spheres to use them as probes in systematic random sampling schemes aimed at achieving length estimates (Fig 2B). The intersections between the isotropic surface of the sphere with the axons are counted, and the resulting number is used to estimate the total length under the conditions of randomness and isotropy above stated. The relevant parameters used in this estimation are the step distance (distance between the spheres in X and Y axes, which determines the number of spheres), and the sphere diameter (which determines the sampling surface dimensions).

To evaluate the efficiency of this method to estimate axon length, we performed sampling with virtual spheres on the cells in the dataset using different combinations of step distance and sphere diameter (Fig 6). The results show that the mean absolute error in the length estimation when using this approach was surprisingly high, reaching values of 60–70% across all

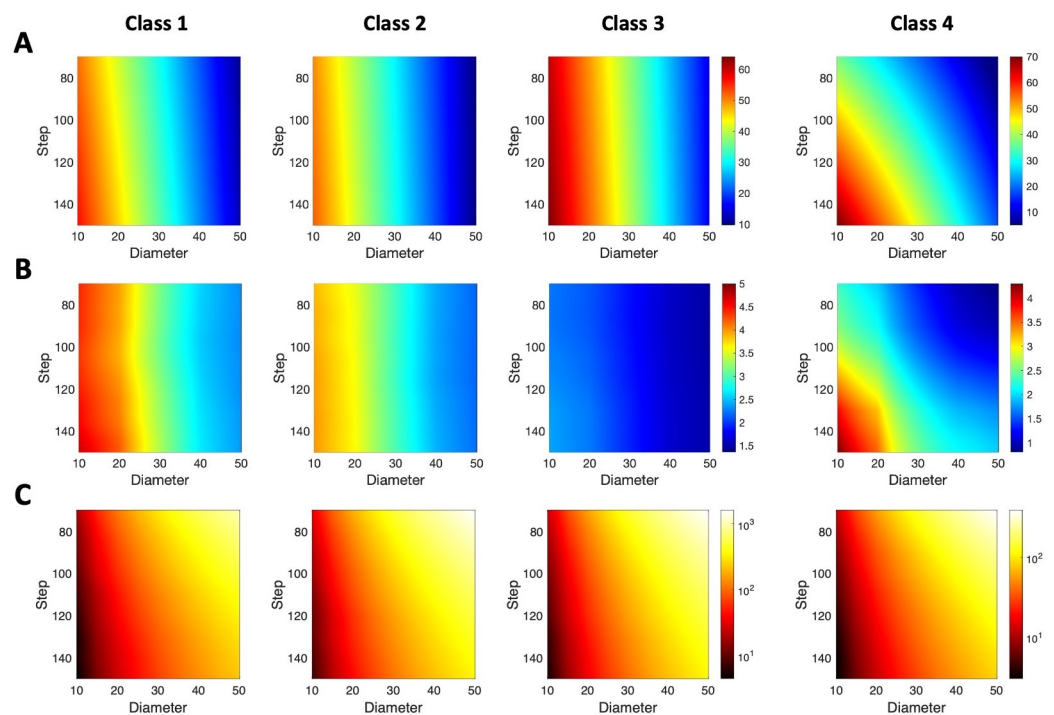


Fig 6. Mean absolute error for axon length estimation by spheres-based stereology. A. The mean absolute error (in % of the real axon length indicated by colors—see color bar) is shown for different values of the probe diameters and the step between sampling boxes, and for axon classes 1 to 4 (columns). Note that the color bar is the same for classes 1, 2, and 3. B. Accuracy of the mean error estimation as maximum error estimation at 95% confidence (in % of the real axon length indicated by colors; same color bar for classes 1, 2, and 3). C. Mean effort, quantized by the mean number of intersections, required to estimate the axon length with different values of the probe diameter and the step for axon classes 1 to 4. Colors denote the number of intersections (in logarithmic scale; same color bar for classes 1, 2, and 3). Mean intersection values were obtained through linear interpolation from estimation for diameter values in 10, 15, 20, . . ., 50 μm and step values in 70, 80, . . ., 150 μm .

<https://doi.org/10.1371/journal.pcbi.1009051.g006>

classes (Fig 6A). In neuron classes 1, 2 and 3 the mean absolute error mainly depends on the probe diameter, being nearly independent of the step size. This is a consequence of using small spheres compared with the axon length. On the contrary, in class 4 (local) neurons, whose axons are significantly smaller than the other classes (Fig 1), the mean absolute error in the axon length estimation showed a dependence on both the sphere diameter and the step size. The accuracy of the mean error estimation (Fig 6B) varies among axon classes, being lower in class 3 due likely to the higher homogeneity in their axonal morphology.

In stereology the estimation error must be balanced with the sampling effort, which results from counting large numbers of intersections between the surface probe and the linear axon. Thus, we quantify the sampling effort directly as the number of intersections. Fig 6C illustrates the mean effort of estimating axon length when using spherical probes, for the different classes analyzed. It shows that for classes 1, 2 and 3, achieving the lowest possible mean absolute error required counting between 200 and more than 1000 intersections, depending on the step size employed during the sampling (the higher the step, the lower the effort). This holds too for class 4 neurons, but the efforts required in general were significantly lower (50–250).

Therefore, Fig 6 is intended to estimate the parameter configuration according to the accuracy-effort trade-off. For instance, in case we would like to estimate the axon length of a class 1 single neuron by means of spheres-based stereology by only accepting a mean error lower than 10% and a mean effort lower than 300 intersections, matching Fig 6A and 6C would suggest the probe diameter equal to 50 and the step higher than 140.

Stereological sampling with virtual planes to estimate 3D length

Other than spheres, it's also possible to stereologically estimate the length of objects using isotropic (i.e., with random orientation) virtual planes as probes [27]. In this case, the sampling is performed in nearly the same way: sampling boxes containing the isotropic planes are spaced at a given XY step to randomly and systematically sample the tissue. The only difference is the introduction of the distance between planes inside the box instead of the diameter of the spheres as the second parameter critical for the stereological estimate (Fig 2C).

The results of estimating axon length through sampling with isotropic virtual planes are depicted in Fig 7. Depending on the combination of XY step and distances used, the mean absolute error for the estimation could be lower than 5% for classes 1–3 and 10% for class 4. The best results were obtained when trying to maximize the sampling surface, that is, when combining small XY steps (80 μm) with small inter-plane distances (5 μm ; Fig 7A), at the cost of increasing the number of intersections. As in the sphere-based axon length estimation, the accuracy of the mean error estimation for virtual planes varies among axon classes (Fig 7B), but it is shown that stereology based on virtual planes is, on average, more accurate than that based on virtual spheres.

The number of intersections was again used to quantify the effort demanded by the stereological procedure (Fig 7C), since performing estimations with low mean absolute errors could require counting abnormally high numbers of intersections. However, specific combinations of parameters could also greatly reduce the mean effort while preserving an acceptable estimation error. For example, when estimating length for class-2 axons, small steps combined with high inter-plane distances produced similar errors at a significantly lower effort cost than small steps combined with small inter-plane distances. This way, by combining Fig 7A and 7C, an estimation of parameter configuration for plane-based stereology could be obtained according to the required mean error and effort.

Results in Fig 7 show the expected estimation error under different parameter combinations. Nonetheless, to make a right choice of XY step and plane distance, the researcher

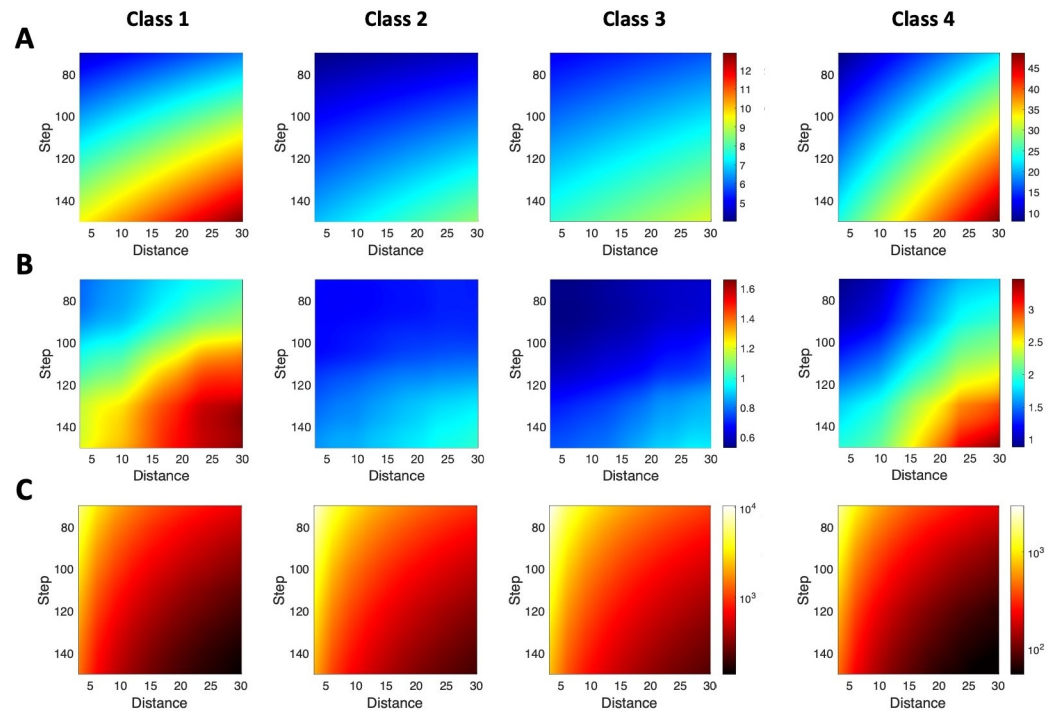


Fig 7. Mean absolute error for axon length estimation by planes-based stereology. A. The mean absolute error (in % of the real axon length indicated by colors—see color bar) is shown for different values of the distance between planes and the step between sampling boxes, and for axon classes 1 to 4 (columns). Note that the color bar is the same for classes 1, 2, and 3. B. Accuracy of the mean error estimation as maximum error estimation at 95% confidence (in % of the real axon length indicated by colors; same color bar for classes 1, 2, and 3). C. Mean effort, quantized by the mean number of intersections, required to estimate the axon length with different values of the distance between planes and the step for axon classes 1 to 4. Colors denote the number of intersections (in logarithmic scale; color bar is the same for classes 1, 2, and 3). Mean intersection values were obtained through linear interpolation from estimation for distance values in 3, 6, 9, . . ., 30 μm and step values in 70, 80, . . ., 150 μm .

<https://doi.org/10.1371/journal.pcbi.1009051.g007>

requires to know the probability of making a certain error under such parameters. This is detailed in Fig 8, which shows the probability of attaining absolute estimation errors lower or equal to 5% (first row in Fig 8A) and 10% (second row in Fig 8A). To easily understand these distribution plots, Fig 8B shows a particular example, denoted for each axon class by white dots in Fig 8A. This example corresponds to a distance = 18 μm and step = 110 μm , and the two areas under each curve quantify the absolute error probability under or equal to 5% and 10% (color areas coincide with the color codes for the corresponding white dots). For instance, for class 1, error probability is equal to 0.39/0.68 (upper/lower panels in A; blue/green areas in first panel in B). That means if the researcher would estimate 100 samples with distance = 18 μm and step = 110 μm , in 35/68 samples the absolute error between real and estimated axon length will be below 5%/10%.

Implementation in the laboratory of the three length estimation methods

In order to illustrate and motivate the discussion about the practical implementation of the tools computationally analyzed here, we measured and estimated the axonal length of six neurons corresponding to the first three axonal classes considered in the study (no class 4 neurons were analyzed) by implementing in the laboratory the same approaches that were used in the computational analysis: 1) direct 3D reconstruction of the axon in NeuroLucida, 2) the projection-based method performed with a camera lucida, and 3) sampling with virtual planes

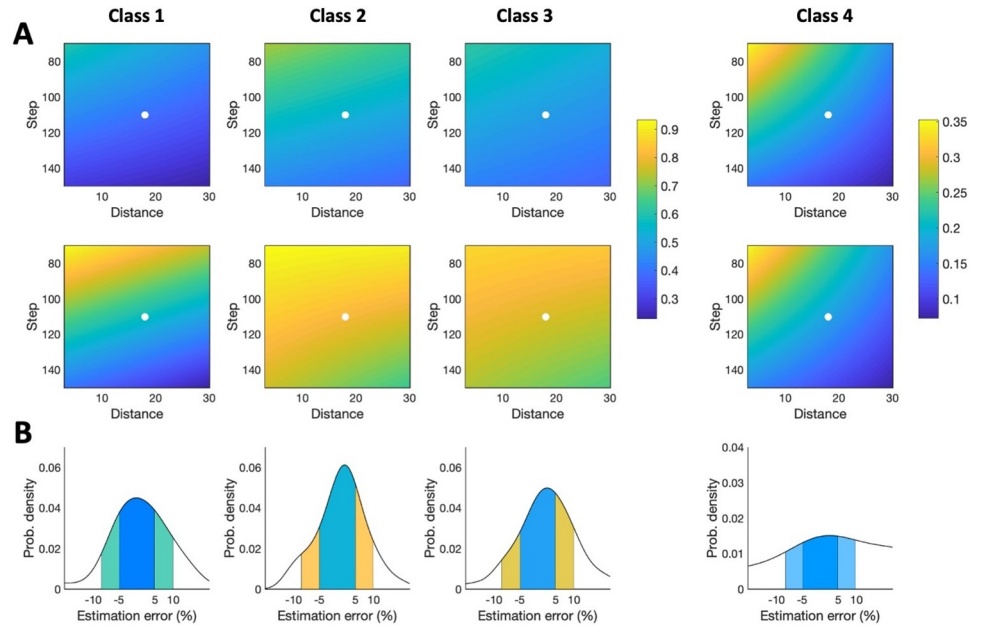


Fig 8. Error probability distribution for axon length estimation by planes-based stereology. A. Probability of $\pm 5\%$ (first row) and $\pm 10\%$ (second row) axon length estimation error for different combinations of distance and step, and for axon classes 1 to 4 (columns); probability is marked by color gradient, from 0.25 to 0.92 (see color bar). Probabilities for classes 1, 2, and 3 are plotted with the same colored-scale. White dots point to the cases for distance = 18 μ and step = 110 μ . Values were obtained through linear interpolation (Adjusted R-squared for 5% error: class 1 = 0.80, class 2 = 0.86, class 3 = 0.81, class 4 = 0.91; Adjusted R-squared for 10% error: class 1 = 0.83, class 2 = 0.83, class 3 = 0.85, class 4 = 0.93). B. Error probability distribution for the particular cases detailed in A. The areas below the curves are the probabilities shown in A and pointed with the white dots.

<https://doi.org/10.1371/journal.pcbi.1009051.g008>

(See [Material and Methods](#)). Results about expected errors comparing the axonal length obtained by the three methods are summarized in [Table 1](#). These results illustrate how implementing these methods in actual tissue entails difficulties that impact on the accuracy of the estimated axonal length. For instance, although the projection-based method proved to be a robust and accurate tool in the computational analysis, its practical implementation resulted in an expected error higher than the one obtained with stereology (11.81% vs 7.48% mean expected error). The possible sources of bias when the analyzed tools are applied in laboratory conditions will be discussed later in light of the axonal length estimations here obtained.

Table 1. Differences between the three axonal length estimation methods after their practical implementation.

	Direct measurement (NeuroLucida)	Projection-based estimation	Stereology (Virtual planes)		
		Expected error	Sections analyzed / Intersections	Experimental error (CE)	Expected error
Class 1 neurons	28162 μ m	35980 μ m (27.76%)	26/834	0.036	28770 μ m (2.16%)
	27855 μ m	22842 μ m (18.00%)	13/304	0.066	24663 μ m (11.46%)
Class 2 neurons	60388 μ m	53301 μ m (11.74%)	31/593	0.043	66712 μ m (10.47%)
	58049 μ m	57755 μ m (0.51%)	7/244	0.067	54900 μ m (5.42%)
	78062 μ m	68526 μ m (12.22%)	10/398	0.053	71640 μ m (8.23%)
Class 3 neuron	44393 μ m	44684 μ m (0.66%)	24/525	0.048	41211 μ m (7.17%)

Stereological parameters: step length X-Y: 75 μ m, plane distance: 5 μ m; CE: coefficient of error.

<https://doi.org/10.1371/journal.pcbi.1009051.t001>

Discussion

We have directly tested and compared, for the first time, the accuracy and reliability of three indirect methods for length estimation of individually labeled axons visualized on serial tissue sections: 1) stereological sampling with virtual spheres [28]; 2) stereological sampling with isotropic virtual planes [27]; 3) and the correction for 2D-projected length in camera lucida drawings [23]. Using the length derived from each neuron's 3D reconstruction as true value, we estimated each method's accuracy or "trueness" as the closeness of agreement between the reference values and the test results. To determine if these three methods yield equally consistent results across a wide range of branching complexity and dispersion, we applied them on axons of four different cell classes [37]. This analysis was performed first computationally, modeling the methods in Matlab and testing them against a dataset of mouse brain neurons from [NeuroMorpho.org](https://neuro.morpho.org), and then on a number of single, thalamocortical cells labeled in serial brain tissue sections from our lab. We conclude that estimations based on stereological sampling with virtual planes or with the 2D projection-based method are a feasible and efficient alternative to complete tracing to estimate axonal length, and that they could be reliably applied to long-range projection neurons. The performance of the three methods is largely consistent over a wide range of axon branching complexity and dispersion.

The projection-based method has been used to estimate the axonal length of single thalamocortical and nigrostriatal cells labeled on histological sections [2,7,23]. This method consists in tracing the axons present in successive sections (using camera lucida or directly from scanned images) and then multiplying the 2D-length measurements by a factor to estimate the real length of the axon (Fig 2). The theoretical value of such a factor depends on the dimension of the embedding space: if the axon is embedded in 3D (2D) and projected onto a plane (line), the factor value is $4/\pi$ ($\pi/2$) (S1 Text). However, the actual suitability of this factor has never been tested against a large number of morphologically diverse neurons. Importantly, for this factor to be accurate, axonal length has to be isotropically distributed (with uniformly distributed orientation, [23]), something that cannot be known beforehand. Here, we used a dataset of 951 neurons of different morphologies to determine the best-fit factor, which for all neuron classes (around 1.27 for classes 1–3). The results of this estimation were consistent across the three orthogonal planes for every class but class 4 (local) neurons, which showed higher errors, presumably due to their smaller size and anisotropic distribution. Thus, our computational approach demonstrates the robustness of the projection-based method independently of the orientation of the plane of section, which provides accurate length estimations with a large sample of heterogeneous axonal architectures.

Design-based stereological methods can also be applied to the specific problem. However, careful selection of sampling parameters is key to make the process efficient while keeping a reasonable accuracy. As a general rule, the more exhaustive the sampling scheme (i.e., counting more intersections between the probe and the object of interest), the more precise the stereological estimation, which will in turn produce lower coefficients of error [39]. Accuracy, on the other hand, depends on the randomness of the sampling process. Although both virtual planes and spheres are based on the same principle [40], the computational results proved the first to be more accurate than the last due to restrictions imposed by the tissue thickness on the sphere's diameter, which resulted in an inefficient and biased sampling and, consequently, a low accuracy. In this sense, large spheres (50 μm in diameter) would not get enough intersections to produce mean absolute errors below 10% when considering sections 50 μm -thick. In the case of virtual planes, accuracy depended on both the XY step (or distance between sampling boxes) and the inter-plane distance, and the results differed slightly between neuron classes: because of their smaller size and their focal and dense architectures, class 1 neurons

required a more intense sampling than neurons in classes 2 and 3 to achieve similar mean absolute errors. Also, the range of mean absolute errors for the virtual planes method was significantly smaller than that for virtual spheres (5–12% vs 10–60%). Thus, although both virtual planes [30,31] and virtual spheres [32–34] have been applied to estimate length in axonal arborizations arising from neuronal populations, when considering single cells in serial sections, the use of virtual planes would be preferable [34].

To corroborate the observations made with the models, the projection-based method and the stereological sampling with virtual planes were tested against six sets of tissue sections, each set containing one single thalamocortical cell of classes 1–3 that had been manually reconstructed in NeuroLucida. Class 4 neurons were excluded, and virtual spheres were not considered for this test because of the inaccurate results they displayed in the previous computational analysis. Virtual planes were applied using a selection of parameters derived from Figs 7 and 8, and the results showed an average expected error of 7.48%, well within the range of what we had previously determined. In addition, sampling error coefficients were also small. The projection-based method, however, didn't translate so well to the real test cases, and its practical implementation resulted in an error that was higher than expected (11.81% in average, but as high as 27% for class 1). We hypothesize that this difference might be attributable to 1) practical biases related to the process of manual tracing with the camera lucida and 2) that these randomly-picked neurons overlap classes 1 and 4. Regarding the first bias, overlapping axons could occlude each other during sampling (especially in dense and focal class 1 neurons). Thus, despite the robustness shown in the computational analysis, the accuracy of the projection-based method suffered when it was implemented in real cases. It should be noted that the axon length estimation by projection is grounded on the zero-anisotropy condition for the axon (S1 Text). The axon of class 1 neurons exhibits one single relevant unbranched subunit, which will introduce a bias in the anisotropy because of its main direction. Thus, it is expected that in class 1 axon anisotropy is further from zero than in the axon of class 2 and 3 neurons, where the existence of two or more unbranched subunits could contribute to balance the final anisotropy. These differences in the fulfillment of the zero-anisotropy condition are illustrated in the absolute error probability for the projection method depicted in Fig 5, where low-error probabilities are less frequent for class 1 than for classes 2 and 3. The impact of real implementation biases on the performance of estimation methods should be experimentally assessed in the future, which would require the labeling, reconstruction and analysis of at least 70 neurons (necessary minimum sample size for an accuracy of the estimation of 5% over slope mean, i.e. maximum possible error of the mean value estimate, calculated at a 95% confidence, estimated from the values of the mean slope and the standard errors obtained from the computational analysis).

Ultimately, the selection of the most suitable method may involve other practical factors, summarized in Table 2. When considering the accuracy of the axon length estimation method, class 1, 2 and 3 neurons can be analyzed with both plane-based stereology and the projection-based method to get acceptable errors. On the other hand, the small size of class 4 neurons allows their fast whole reconstruction, so no estimation methods are required to study their axonal (and dendritic) morphology.

In terms of economic cost, for example, the most accessible of the three methods is the projection-based approach, since it only requires a camera lucida/imaging system attachment for a microscope and a computer system with basic graphic design software. If a higher throughput and accuracy is required, the microscope could then be substituted with a slide scanner. However, this would raise the cost and make it similar to that of the specific software tools required to carry out design-based stereology (VIS or Stereo Investigator) or 3D, manual, direct reconstruction (NeuroLucida). The projection-based approach requires less training,

Table 2. Comparison of methodological approaches to measure or estimate axonal length in single neurons.

Method	Key system requirements	Cost	Training requirements	Time	Method Biases	Expected error range	Other Outputs	
3D reconstruction (direct measurement)	NeuroLucida	XYZ stage NeuroLucida	++	++	+++	++	Reference value	3D model
	Semi-automatic reconstruction (MouseLight)	Two-photon microscope with vibratome	+++	++	+	+		
Projections (model-based estimation)	Correction of 2D length	Camera lucida	+	+	++	+++	class 1: [1.6, 6.9] class 2: [1.0, 4.7] class 3: [1.1, 6.2]	2D model
		Slide-scanner	++	+	+	++		
Stereology (design-based estimation)	Space Balls	XYZ stage Stereology software	++	+++	+	+	class 1: [10.7, 56.8] class 2: [9.7, 52.4] class 3: [15.3, 64.1]	None
	Virtual Planes	XYZ stage Stereology software	++	+++	+	+		

<https://doi.org/10.1371/journal.pcbi.1009051.t002>

and also produces a 2D model of the neuron. 3D tracing is also relatively easy to learn and implement, whereas design-based stereology is the most complex of the three, requiring extensive know-how about sampling design or the advice of an expert. In this regard, **Figs 6 and 7** can provide some insights that help to design the stereological procedure when using either spheres or plane probes. Thus, the choice of the adequate parameters, i.e. distance between probes and sampling intensity, will depend on the class of neuron analyzed, and aims to get the highest efficiency, which means the less analysis time to get a low error estimation (around 5%). In the case of virtual planes, class 1 neurons, which normally have short and focalized axons, need more sampling intensity than classes 2 and 3 to get the same error estimation (comparison between panels 7A and 7C for the same parameter values); the opposite happens with class 4 neurons in virtual spheres, that requires less effort (less sampling intensity) than the other neuron classes to get the same error estimations.

With regards to efficiency, the three methods have in common the same disadvantage: they require sparsely-labeled brains (i.e., containing only a few labeled cells that don't overlap, to avoid errors in the reconstruction). Otherwise, axons from different neurons overlapping each other could be difficult or even impossible to distinguish from one another. With that in mind, the time required to quantify the axon length of a single neuron naturally depends on its size and spread, and more so in the case of manual 3D tracing. Whereas design-based stereology and the projection-based approach can analyze a large and complex mouse axon in about 8–16 hours, manually tracing that same cell in NeuroLucida could take 10 times more. Still, the main advantage of direct reconstructions is that they also produce a 3D model of the neuron, with a collection of geometrical and topological parameters to be extracted from its structure, other than just length.

Finally, potential biases are associated with each specific method. In fact, not even direct 3D reconstruction-tracing methods, which we took as in this study, are totally free of them. The implementation of any of these methods, therefore, has to rely on clear and reproducible

criteria, so as to reduce inter-individual differences between researchers when counting intersections, in the case of stereology, or tracing axons, in the case of reconstructions [41]. Also, magnification has to be relatively high ($\geq 200\times$), so that individual branches are clearly recognizable as such. The greatest variation in the results is, perhaps, that introduced by the shrinkage suffered by the sections due to histological processing. Fixation procedures with paraformaldehyde and sucrose cryoprotection of the brain can introduce a shrinkage of around 15% in all dimensions, whereas the dehydration process with alcohol prior to tissue covering on the slide are known to introduce a shrinkage of up to 70% in the Z axis (therefore reducing the section thickness [42]). This shrinkage correction has to be properly applied in measurements derived from both NeuroLucida and the design-based stereological approaches; otherwise, length will be underestimated. In the case of the projection-based approach, this correction is not necessary, given that it relies on 2D (XY) length, effectively ignoring the Z-dimension.

The current gold-standard in both resolution and throughput for this kind of studies are the large-scale pipelines developed by initiatives in the Allen Institute and the MouseLight projects [6,20,21], which are producing hundreds of neuron reconstructions registered on a template atlas in a semi-automatic manner. However, their specific requirements make them suitable to only a small number of highly-funded research centers. The methods discussed above, therefore, offer a reasonable alternative when working with sparsely labeled brains. Therefore, the majority of research groups without access to these tools can consider the methods discussed in this paper to fulfill their own research goals.

In conclusion, accurate measurement of individual axon length is crucial as this feature is an accessible estimation of the functional impact of the single neuron. Nonetheless, the technical and economic difficulties of direct axon length measurement urge for accurate, but less time and effort demanding length estimations. The three approaches presented here—projection-based length estimation, stereology, and direct measurements from reconstructions—are valid for generating accurate axonal length estimations of single cells. The stereological method is less prone to biases inherent to the manual drawing of fibers in camera lucida projection-based estimations. Among the two stereological approaches, the virtual planes method is more efficient and accurate than the one using spheres when dealing with single cell axons. Informed by the morphometric evidence presented here, the choice between these methods may thus largely depend on the human effort, training required for know-how acquisition, and economic cost. We therefore provide a useful guide for selecting the most appropriate individual axon length estimation method and the best parameters regarding the axonal morphology. Our results could be an important reference for neuroscientists interested in the wiring of neuronal circuits with powerful single-cell resolution methods, and in the building of brain models derived from this new anatomical knowledge.

The advantages and disadvantages of the three methods here discussed have been summarized in Table 2 in terms of cost, training time, time of analysis, possible biases, the possibility of extracting additional information beyond the axonal length, and the error range obtained computationally for neuron classes 1, 2, and 3. Different colors (green = positive: low/affordable/easy; red = negative: high/expensive/hard; yellow: intermediate) and +, ++ or +++ stand for different levels in each of the parameters considered. Cost: +, ~ 10.000\$; ++, affordable according to average European grant support (~ 50.000\$); +++, restricted to research centers specialized in single neuron reconstruction. Training requirements: +, one day of training approximately and no previous experience required (basic microscope knowledge to trace axons in 2D); ++, two days of training (tracing axons in 3D with either NeuroLucida or equivalent software); +++, an expert in stereology is needed to perform the sampling design. Analysis time (per neuron): +, around 8–16 h/neuron including slide scanning and digital tracing for

projection-based, tracing for semi-automatic methods and counting intersections and data analysis for stereology; ++, around 20–25 h/neuron including manual tracing, scanning and digital tracing; +++, between 50–100 h. Note that the time analysis depends on density and length of the neuron (class 1 analysis is faster than class 2 and 3 analysis for all methods here studied). Potential method biases: tissue shrinkage not being properly corrected affects to stereology and NeuroLucida; difficulties in identification of axons due to staining problems would affect to all methods; interindividual differences in the level of drawing precision affects especially to NeuroLucida and camera lucida reconstruction (proper magnification should be used in this sense $\geq 200\times$); camera lucida tracing is especially sensitive to axon overlapping in profuse arbors.

Supporting information

S1 Text. Mathematical derivation of the coefficient relating the lengths of the real axon and its 2D projection.

(DOCX)

Acknowledgments

We thank Dr. Avendaño-Trueba for his advice on the approach and the development of this project and Marta Callejo-Mostoles for her excellent technical assistance during tissue processing.

Author Contributions

Conceptualization: Mario Rubio-Teves, Sergio Díez-Hermano, César Porrero, Abel Sánchez-Jiménez, Francisco Clascá, María García-Amado, José Antonio Villacorta-Atienza.

Data curation: Sergio Díez-Hermano, José Antonio Villacorta-Atienza.

Formal analysis: Mario Rubio-Teves, Sergio Díez-Hermano, César Porrero, Abel Sánchez-Jiménez, María García-Amado, José Antonio Villacorta-Atienza.

Funding acquisition: Sergio Díez-Hermano, Lucía Prensa, Francisco Clascá.

Investigation: Mario Rubio-Teves, Sergio Díez-Hermano, César Porrero, Abel Sánchez-Jiménez, María García-Amado, José Antonio Villacorta-Atienza.

Methodology: Mario Rubio-Teves, Sergio Díez-Hermano, César Porrero, Abel Sánchez-Jiménez, María García-Amado, José Antonio Villacorta-Atienza.

Project administration: María García-Amado, José Antonio Villacorta-Atienza.

Software: Sergio Díez-Hermano, José Antonio Villacorta-Atienza.

Writing – original draft: Mario Rubio-Teves, Sergio Díez-Hermano, María García-Amado, José Antonio Villacorta-Atienza.

Writing – review & editing: Mario Rubio-Teves, Sergio Díez-Hermano, César Porrero, Lucía Prensa, Francisco Clascá, María García-Amado, José Antonio Villacorta-Atienza.

References

1. Furuta T, Tomioka R, Taki K, Nakamura K, Tamamaki N, Kaneko T. In vivo transduction of central neurons using recombinant Sindbis virus: Golgi-like labeling of dendrites and axons with membrane-targeted fluorescent proteins. *Journal of Histochemistry & Cytochemistry*. 2001; 49(12), 1497–1507. <https://doi.org/10.1177/002215540104901203> PMID: 11724897

2. Kuramoto E, Furuta T, Nakamura KC, Unzai T, Hioki H, Kaneko, T. Two types of thalamocortical projections from the motor thalamic nuclei of the rat: a single neuron-tracing study using viral vectors. *Cerebral cortex*. 2009; 19(9), 2065–2077. <https://doi.org/10.1093/cercor/bhn231> PMID: 19174446
3. Cazemier JL, Clascá F, Tiesinga PH. Connectomic analysis of brain networks: Novel techniques and future directions. *Frontiers in neuroanatomy*. 2016; 10, 110. <https://doi.org/10.3389/fnana.2016.00110> PMID: 27881953
4. Economo MN, Clack NG, Lavis LD, Gerfen CR, Svoboda K, Myers EW, Chandrashekar J. A platform for brain-wide imaging and reconstruction of individual neurons. *Elife*. 2016; 5, e10566. <https://doi.org/10.7554/eLife.10566> PMID: 26796534
5. Porrero C, Rodríguez-Moreno J, Quetglas JI, Smerdou C, Furuta T, Clascá F. A simple and efficient in vivo non-viral RNA transfection method for labeling the whole axonal tree of individual adult long-range projection neurons. *Frontiers in neuroanatomy*. 2016; 10, 27. <https://doi.org/10.3389/fnana.2016.00027> PMID: 27047347
6. Winnubst J, Bas E, Ferreira TA, Wu Z, Economo MN, Edson P, et al. Reconstruction of 1,000 projection neurons reveals new cell types and organization of long-range connectivity in the mouse brain. *Cell*. 2019; 179(1), 268–281. <https://doi.org/10.1016/j.cell.2019.07.042> PMID: 31495573
7. Kuramoto E, Pan S, Furuta T, Tanaka YR, Iwai H, Yamanaka A, et al. Individual mediodorsal thalamic neurons project to multiple areas of the rat prefrontal cortex: A single neuron-tracing study using virus vectors. *Journal of Comparative Neurology*. 2017; 525(1), 166–185. <https://doi.org/10.1002/cne.24054> PMID: 27275581
8. Ohno S, Kuramoto E, Furuta T, Hioki H, Tanaka YR, Fujiyama F, et al. A morphological analysis of thalamocortical axon fibers of rat posterior thalamic nuclei: a single neuron tracing study with viral vectors. *Cerebral cortex*. 2012; 22(12), 2840–2857. <https://doi.org/10.1093/cercor/bhr356> PMID: 22190433
9. Rodríguez-Moreno J, Porrero C, Rollenhagen A, Rubio-Teves M, Casas-Torremocha D, Alonso-Nanclares L, et al. Area-specific synapse structure in branched posterior nucleus axons reveals a new level of complexity in thalamocortical networks. *Journal of Neuroscience*. 2020; 40(13), 2663–2679. <https://doi.org/10.1523/JNEUROSCI.2886-19.2020> PMID: 32054677
10. Stuart GJ, Spruston N. Dendritic integration: 60 years of progress. *Nature neuroscience*. 2015; 18(12), 1713–1721. <https://doi.org/10.1038/nn.4157> PMID: 26605882
11. Villacorta-Atienza JA, Castro J, Negredo P, Avendaño C. Mathematical foundations of the dendritic growth models. *Journal of Mathematical Biology*. 2007; 55 (5–6), 817–859. <https://doi.org/10.1007/s00285-007-0113-7> PMID: 17646989
12. Stepanyants A., Hof P. R., & Chklovskii D. B. (2002). Geometry and structural plasticity of synaptic connectivity. *Neuron*, 34(2), 275–288. [https://doi.org/10.1016/s0896-6273\(02\)00652-9](https://doi.org/10.1016/s0896-6273(02)00652-9) PMID: 11970869
13. Nielsen MA. *Neural networks and deep learning*. San Francisco, CA: Determination press; 2015.
14. Rolls ET, Treves A, Rolls ET. *Neural networks and brain function* (Vol. 572). Oxford: Oxford university press; 1998.
15. Villacorta-Atienza JA, Makarov V. Neural Network Architecture for Cognitive Navigation in Dynamic Environments. *IEEE Transactions on Neural Networks and Learning Systems*. 2013; 24(12), 2075–2087. <https://doi.org/10.1109/TNNLS.2013.2271645> PMID: 24805224
16. Rodríguez-Moreno J, Rollenhagen A, Arlandis J, Santuy A, Merchán-Pérez A, DeFelipe J, et al. Quantitative 3D ultrastructure of thalamocortical synapses from the “lemniscal” ventral posteromedial nucleus in mouse barrel cortex. *Cerebral Cortex*. 2018; 28(9), 3159–3175. <https://doi.org/10.1093/cercor/bhx187> PMID: 28968773
17. Markram H, Muller E, Ramaswamy S, Reimann MW, Abdellah M, Sanchez CA, et al. Reconstruction and simulation of neocortical microcircuitry. *Cell*. 2015; 163(2), 456–492. <https://doi.org/10.1016/j.cell.2015.09.029> PMID: 26451489
18. Iavarone E, Yi J, Shi Y, Zandt BJ, O'Reilly C, Van Geit W, et al. Experimentally-constrained biophysical models of tonic and burst firing modes in thalamocortical neurons. *PLoS Comput Biol*. 2019; 15(5): e1006753. <https://doi.org/10.1371/journal.pcbi.1006753> PMID: 31095552
19. Zeng H, Sanes JR. Neuronal cell-type classification: challenges, opportunities and the path forward. *Nature Reviews Neuroscience*. 2017; 18(9), 530. <https://doi.org/10.1038/nrn.2017.85> PMID: 28775344
20. Lin HM, Kuang JX, Sun P, Li N, Lv X, Zhang YH. Reconstruction of intratelencephalic neurons in the mouse secondary motor cortex reveals the diverse projection patterns of single neurons. *Frontiers in neuroanatomy*. 2018; 12, 86. <https://doi.org/10.3389/fnana.2018.00086> PMID: 30425624
21. Phillips JW, Schulmann A, Hara E, Winnubst J, Liu C, Valakh V, et al. A repeated molecular architecture across thalamic pathways. *Nature neuroscience*. 2019; 22(11), 1925–1935. <https://doi.org/10.1038/s41593-019-0483-3> PMID: 31527803

22. Morita K, Im S, Kawaguchi Y. Differential striatal axonal arborizations of the intratelencephalic and pyramidal-tract neurons: analysis of the data in the MouseLight Database. *Frontiers in Neural Circuits*. 2019; 13, 71. <https://doi.org/10.3389/fncir.2019.00071> PMID: 31803027
23. Matsuda W, Furuta T, Nakamura KC, Hioki H, Fujiyama F, Arai R, et al. Single nigrostriatal dopaminergic neurons form widely spread and highly dense axonal arborizations in the neostriatum. *Journal of Neuroscience*. 2009; 29(2), 444–453. <https://doi.org/10.1523/JNEUROSCI.4029-08.2009> PMID: 19144844
24. Parekh R, Ascoli GA. Neuronal morphology goes digital: a research hub for cellular and system neuroscience. *Neuron*. 2013; 77(6), 1017–1038. <https://doi.org/10.1016/j.neuron.2013.03.008> PMID: 23522039
25. Aguiar P, Sousa M, Szucs P. Versatile morphometric analysis and visualization of the three-dimensional structure of neurons. *Neuroinformatics*. 2013; 11(4), 393–403. <https://doi.org/10.1007/s12021-013-9188-z> PMID: 23765606
26. Oberlaender M, de Kock CP, Bruno RM, Ramirez A, Meyer HS, Dercksen VJ, et al. Cell type-specific three-dimensional structure of thalamocortical circuits in a column of rat vibrissal cortex. *Cerebral cortex*. 2012; 22(10), 2375–2391. <https://doi.org/10.1093/cercor/bhr317> PMID: 22089425
27. Larsen JO, Gundersen HJ, Nielsen J. Global spatial sampling with isotropic virtual planes: estimators of length density and total length in thick, arbitrarily orientated sections. *Journal of Microscopy*. 1998; 191(3), 238–248. <https://doi.org/10.1046/j.1365-2818.1998.00365.x> PMID: 9767488
28. Mouton PR, Gokhale AM, Ward NL, West MJ. Stereological length estimation using spherical probes. *Journal of microscopy*. 2002; 206(1), 54–64. <https://doi.org/10.1046/j.1365-2818.2002.01006.x> PMID: 12000563
29. Calhoun ME, Mouton PR. Length measurement: new developments in neurostereology and 3D imagery. *Journal of chemical neuroanatomy*. 2000; 20(1), 61–69. [https://doi.org/10.1016/s0891-0618\(00\)00074-0](https://doi.org/10.1016/s0891-0618(00)00074-0) PMID: 11074344
30. Casas-Torremocha D, Porrero C, Rodríguez-Moreno J, García-Amado M, Lübke JH, Núñez A, et al. Posterior thalamic nucleus axon terminals have different structure and functional impact in the motor and somatosensory vibrissal cortices. *Brain Structure and Function*. 2019; 224(4), 1627–1645. <https://doi.org/10.1007/s00429-019-01862-4> PMID: 30919051
31. García-Amado M, Prensa L. Distribution of dopamine transporter immunoreactive fibers in the human amygdaloid complex. *European J Neurosci*. 2013;38. <https://doi.org/10.1111/ejn.12358> PMID: 24102648
32. Monje MHG, Blesa J, García-Cabezas MA, Obeso JA, Cavada C. Changes in thalamic dopamine innervation in a progressive Parkinson's disease model in monkeys. *Mov Disord*. 2020; 35(3):419–430. <https://doi.org/10.1002/mds.27921> PMID: 31800134
33. Jiménez-Sánchez L, Blesa J, Del Rey NL, Monje MHG, Obeso JA, Cavada C. (2020) Serotonergic innervation of the striatum in a nonhuman primate model of Parkinson's disease. *Neuropharmacology*. 2020;170. <https://doi.org/10.1016/j.neuropharm.2019.107806> PMID: 31589886
34. Nikolajsen GN, Jensen MS, West MJ. Cholinergic axon length reduced by 300 meters in the brain of an Alzheimer mouse model. *Neurobiol Aging*. 2011; 32(11):1927–31. <https://doi.org/10.1016/j.neurobiolaging.2011.05.006> PMID: 21752495
35. Aransay A, Rodríguez-López C, García-Amado M, Clascá F, Prensa L. Long-range projection neurons of the mouse ventral tegmental area: a single-cell axon tracing analysis. *Frontiers in neuroanatomy*. 2015; 9, 59. <https://doi.org/10.3389/fnana.2015.00059> PMID: 26042000
36. Ascoli GA, Donohue DE, Halavi M. NeuroMorpho. Org: a central resource for neuronal morphologies. *Journal of Neuroscience*. 2007; 27(35), 9247–9251. <https://doi.org/10.1523/JNEUROSCI.2055-07.2007> PMID: 17728438
37. Clascá F, Porrero C, Galazó MJ, Rubio-Garrido P, Evangelio M. Anatomy and development of multispecific thalamocortical axons: implications for cortical dynamics and evolution. In *Axons and brain architecture* (pp. 69–92). Academic Press; 2016.
38. Drøjdahl N, Nielsen HH, Gardi JE, Wree A, Peterson AC, Nyengaard JR, et al. (2010). Axonal plasticity elicits long-term changes in oligodendroglia and myelinated fibers. *Glia*. 2010; 58(1), 29–42. <https://doi.org/10.1002/glia.20897> PMID: 19455714
39. Gundersen HJ, Jensen EB, Kieu K, Nielsen J. The efficiency of systematic sampling in stereology—reconsidered. *J. Microsc*. 1999; 193, 199–211. <https://doi.org/10.1046/j.1365-2818.1999.00457.x> PMID: 10348656
40. Smith CS, Guttman L. Measurement of internal boundaries in three-dimensional structures by random sectioning. *JOM*. 1953; 5(1), 81–87.

41. Ochs M. The closer we look the more we see? Quantitative microscopic analysis of the pulmonary surfactant system. *Cell Physiol Biochem*. 2010; 25(1), 27–40. <https://doi.org/10.1159/000272061> PMID: [20054142](https://pubmed.ncbi.nlm.nih.gov/20054142/)
42. Dorph-Petersen KA, Nyengaard JR, Gundersen HJ. Tissue shrinkage and unbiased stereological estimation of particle number and size. *J. Microsc.* 2001; 204 (Pt3): 232–246. <https://doi.org/10.1046/j.1365-2818.2001.00958.x> PMID: [11903800](https://pubmed.ncbi.nlm.nih.gov/11903800/)